Contract N00014-77-C-0266

ESTIMATION OF ICE SURFACE SCATTERING AND ACOUSTIC ATTENUATION IN ARCTIC SEDIMENTS FROM LONG-RANGE PROPAGATION DATA

G.L. Duckworth
A.B. Baggeroer

Massachusetts Institute of Technology
Cambridge, MA 02139
U.S.A.

ABSTRACT

A single explosive shot at a range of 341.3 km in the Pole Abyssal Plain of the Arctic Ocean is used to assess the components of propagation loss for this region. The acoustic energy propagated between a satellite ice camp and the Fram II ice station in a water column of nearly uniform depth. Much of the observed energy interacted with the upper 200 meters of sediments along a path which was nearly parallel to the Arctic Mid-Ocean Ridge. In addition, the upward refracting sound channel of the Arctic Ocean also caused the observed energy to interact extensively with the ice canopy, which was contiguous over the entire path. The deterministic lateral homogeneity of the bathymetry and sediments, and the statistical lateral homogeneity of the ice canopy in this region allow us to attempt to separate the effects of geometrical spreading, ice surface scattering, and effective sediment compressional wave attenuation. The primary data for this work are observations of the signal from a 25.9 kg explosive charge received on a 24 channel two-dimensional hydrophone array with a 1 km aperture. The data are inadequate to resolve attenuation at depth, but provide an estimate for frequency independent Q of 200 to 300 for the upper 200 meters of the sediments and a dependency of surface scattering on frequency over the 5-50 Hz band. It is shown that partially coherent summation of the surface multipaths is required to predict the observations.

INTRODUCTION

Discussion

The goal of this paper is to assess the effects of sediment attenuation and surface scattering on acoustic propagation in the Arctic Ocean. A model relating observations, source characteristics, surface scattering, and attenuation for a series of multiple arrivals observed at a constant offset from a single explosion is given in decibels by:

$$P(f,n) = S(f) + R_2(f,n) + G(n) + R_1(f,n) + A(f,n) \qquad (1)$$

where

f	is the temporal frequency in Hz;
n	is the order of the multiple observed;
$P(f,n)$	is the observed data energy spectral density;
$S(f)$	is the source explosion energy spectral density;
$R_2(f,n)$	is the factor accounting for the near source and near receiver reflections and the random travel-time component due to the rough under-ice surface;
$G(n)$	is the geometrical spreading factor;

$R_1(f,n)$ is the amplitude component of surface scattering and ocean bottom transmissions for the linear surface and bottom interactions;

$A(f,n)$ is the attenuation factor due to effective Q along the travel path.

In this equation, the sound speed model is assumed known, so the multiple order, n, completely specifies the turning point depth, z, the ray slowness, p, and the length and time of the travel path in the sediments and water column.

Knowledge of the sound speed in the water column and sediment also specifies the geometrical spreading factor, $G(n)$, for a constant offset. The sound-speed profile is computed from the data separately. We compute $S(f)$ from the well known and regarded empirical spectra of TNT explosions at known depths, and estimate the scattering terms, $R_1(f,n)$, and the attenuation, $A(f,n)$, from the data.

We examine both the Fraunhofer and Fresnel approximations in the identification of under-ice roughness parameters. It is seen that the combination of travel-time fluctuation measurements through $R_2(f,n)$ and amplitude scattering from $R_1(f,n)$ allows characterization of both the rms surface roughness averaged over a Fresnel zone, $\bar{\sigma}_z$, and the instantaneous rms roughness, σ_z.

One assumption that is made, and one that has come under intense scrutiny in recent work [1,2], is an effective sediment quality factor, Q, which is constant over the frequency band from 5 to 50 Hz. For this work, this assumption is necessary in order to separate ice surface scattering effects from attenuation. Our assumptions and experimental geometry also do not allow estimation of Q as a function of multiple, n, and thus of the path integral which a ray follows to its maximum depth. Even if this had been possible, we would not have attempted to invert these estimates for "instantaneous" depth because it is unclear what the result of this inversion may mean. Due to the lack of separation of intrinsic Q from the geometrical effects of layered bedding the Q encountered by a ray at a given depth depends on the direction of the ray with respect to the bedding[2]. It is our feeling that a value of constant Q averaged over all multiples with a maximum depth of penetration of 200 meters is a more reliable quantity, and is consistent with the dominant energy wavelengths of 60-150 meters.

One very important point that will be made is that for propagation distances of 340 km in sediments and water column it is important to retain the coherency of near source and receiver multipaths to predict the spectral shape and amplitude of the received arrivals in the 5-50 Hz band. Though they will not be dealt with in this paper, the incoherent scattering aspects of the propagation may also be treated by analysing the scattered energy observed on our records between the strong arrivals. In this work, however, we will quantify random scattering only through expression as losses from the primarily coherent data. We are able to do this because of our fortuitous location in the nearly laterally invariant Pole Abyssal Plain, and because of the great temporal and spatial stability of the Arctic Ocean[3].

Background

Spectral ratio methods such as those used for this work are quite popular for estimation of attenuation in marine sediments. Stoll and Houtz[2] provide a good bibliography of recent work. This work differs from many of those efforts in that it attempts to separate source directivity effects, surface scattering, bottom transmission, and effective Q in the sediments using both travel-time and amplitude information. In addition, estimates for these parameters in the Arctic are quite sparse. This work should also compliment recent work by Lee and Kutschale[4], which used full-wave forward modeling to determine sediment Q in the Arctic. Their work required the inclusion of a frequency independent Q of 190-220 to obtain the observed dispersion and amplitude characteristics of later arriving sediment interaction multiples in experiments identical to ours. They also assumed that surface scattering was negligible in their frequency band from 5 to 30 Hz.

Experiment Location and Receiver Characteristics

The data used for this work are from the Fram II experiment in the Pole Abyssal Plain of the Arctic Ocean. The shot was initiated at a remote ice camp (Camp 1) at 88.850°N, 18.75°W on 26 April 1980 at 1427 GMT. The data were received at the Fram II base camp drifting with the ice pack at 85.786°N and 24.41°W. This is a great circle distance of 341.3 km at 2° true from the Fram II camp. Bathymetric charts show a water depth of 4-4.3 km along most of the path[4]. This path was nearly parallel to the

spreading center at the Arctic Mid-ocean Ridge and followed magnetic anomaly 24. The constant age and bathymetry along the path predispose us to believe that the sediments are laterally homogeneous. Few samples of the sediment are available, and we assumed the sediments to be turbidites. Other experimental evidence suggests that the assumption of a constant Q with frequency is good for this type of sediment[5,6].

The logistics of this experiment, including the receiving array configuration and recording capabilities are detailed by Duckworth et al.,[7]. For the shot analyzed in this paper, 22 hydrophone recording channels were used in a two-dimensional array configuration over a 1 km aperture. The hydrophone depth was 93 meters. The data are good from 5 Hz to 80 Hz. Below 5 Hz hydrophone strum became a problem, and the digital floating point acquisition system had anti-alias filters at 80 Hz.

Paper Outline

We first discuss the models that will be used to interpret the data. These include the source spectrum, geometrical spreading, near surface reflection characteristics, surface and bottom scattering effects, and the attenuation model. The data processing sequence is outlined, and some of the observational aspects of the data requiring little interpretation are presented. We then present the procedure used to obtain the Q estimate and the model parameters for the scattering loss. Finally, we comment on the reliability, resolution, and interpretation of our results, compare them to previous work, and indicate what further analysis would benefit the goals of this paper.

MODELING

Source

The source was 25 kg of TNT detonated by a depth activated Mk 82 SUS charge (0.8 kg TNT). The TNT explosive charge has been studied extensively as a pressure source in the water column. We implemented the equations of Wakeley[8] and computed a source signature for a depth of 93 meters and received at a range of 1 km. This range introduces some additional nonlinear attenuation of high frequencies over the calculation at 1 meter. This was corrected by +60 dB to obtain the signature at 1 meter, and then by -160 dB to obtain the voltage waveform we would obtain from our -160 dB re $1 V/\mu Pa$ hydrophones. Voltage spectral levels, not pressure, will be used throughout the paper assuming phones of this sensitivity. The waveform was sampled at 10 kHz to catch the high frequency components of the shock wave and passed through a digital filter with an 80 Hz cutoff to mimic our analog anti-alias filter, decimated to a 4 msec sample interval, and its spectrum computed by a padded, unwindowed FFT with appropriate corrections for one-sided energy spectral density re $1 V^2/Hz$. The spectrum was then smeared over a 4 Hz band by a running frequency average to give it the same bandwidth averaging characteristics as our data analysis procedure. The spectrum is shown in Fig. 1 and agrees well with that published by Urick[9].

Geometrical Spreading

Because we are attempting to estimate the scattering losses in absolute terms, rather than just the slope of the spectral ratio to obtain Q[10], it is necessary to compute the geometrical spreading loss. In our model, this is assumed to be independent of frequency and will be computed by ray theory from a laterally invariant sound speed profile for the water column and sediments.

The water column profile was obtained from a combination of direct sound speed measurements, theory, and inversion of the observed water column modal dispersion curves for this shot. The procedure is presented by Duckworth[11 (Chapter 6)]. The

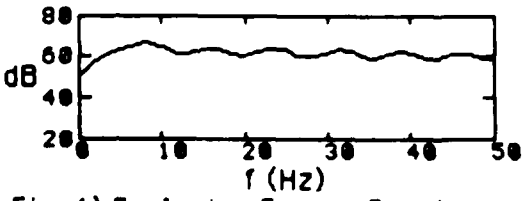

Fig. 1) Explosion Energy Spectrum.

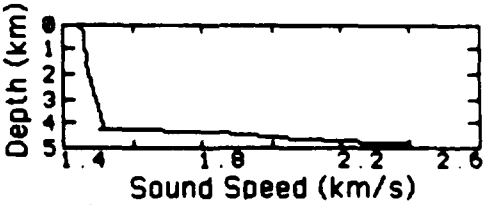

Fig. 2) Sound speed model.

sediment profile was determined by travel-time inversion of $\tau(p)$ and $x(p)$ curves estimated from the data by the methods described by Duckworth et al.[7]. The inversion methods of Diebold and Stoffa[12] and Dorman and Jacobson[13] were used after correcting the array estimated slownesses for slight bathymetric dip local to the receiving array. A preliminary inversion of this type is given by Duckworth[11 (Chapter 6)]. This profile is nearly identical to that of Lee[4]. Lee also found that shear wave conversion was not important for these paths.

The resulting sound speed profile is shown in Fig. 2. All travel times, phase velocities, and geometrical spreading factors were computed using linear velocity gradient segments between speed/depth points specified by this model. The geometric spreading loss assumes a spherically symmetric pressure source and no free surface interaction. The travel times of the data were measured at 8 Hz, the peak energy frequency of the source signature, using travel time detection on the maximum-likelihood beamformed output of the array[11 (Chapter 3)].

Bottom Transmission and Surface Scattering Losses

Bottom Transmission Coefficient: First, and seemingly least important to propagation loss in this area, is the transmission/reflection coefficient at the ocean bottom. Due to the long spatial wavelengths of bottom features in abyssal plains, we model this interaction independent of frequency in our band. Since we are dealing strictly with refracted arrivals, the transmission effects are the only ones to be considered. We feel that this frequency independent term in $R_1(f,n)$ should be very small due to gradual matching between the impedance of the water and the bottom by a very unconsolidated layer of about 35 meters thickness. In this layer the sound speed in the sediments is modeled to drop below that of the water column. Samples of the bottom obtained from OBS units dropped from the Fram II camp support this hypothesis [H.R. Jackson, personal communication, 1984]. Because of the extremely small losses at low frequencies where surface scatter is less important, we find that the bottom reflection coefficient is less than 0.2. This would give a maximum transmission loss of 0.35 dB/multiple, which will be seen to be consistent with our data. Helmberger, et al.[14] found the same bound for deep sediments in the Bering Sea.

Surface Scattering: The pressure of the shock wave at the surface above a 25.8 kg TNT explosion at a slant range of 186 meters is 233 dB re $1\mu Pa$. This is greater than the 222 dB pressure due to the atmosphere and 2 meter water surface suppression by the ice, thus indicating that there may be clipping of the rarefaction peak. However, our observations with low sensitivity monitor phones indicate that no cavitation takes place, and that all losses must be due to scattering from the uneven upper surface of the ice. We could not resolve any reflection from the bottom of the ice with a positive reflection coefficient in observations up to 1 kHz, indicating that a slushy matching layer is in effect here, as well as at the sea bottom. Experiments by Weston[15] indicate that the cavitation threshold in seawater is 246 dB re $1\mu Pa$ for short duration stresses, such as the explosive shock wave, supporting our observations.

If the multipaths shown in Fig. 3 are considered, where any equal number, $(n-1)$, of surface interactions may be present at the breaks in the rays between the source and receiver, then the transfer function due to surface scattering and bottom transmission from the explosion source to that received for the multiple of order n is given by:

$$P(f,n) - S(f) = H(f,n) \tag{2}$$

$$= 10 \log_{10} \left| \left[\alpha_1^{n-1} e^{-i2\pi f \tau_a} + \alpha_2 \alpha_1^{n-1} e^{-i2\pi f \tau_b} + \alpha_1^n e^{-i2\pi f \tau_c} + \alpha_2 \alpha_1^n e^{-i2\pi f \tau_d} \right] \right|^2$$

where

$\tau_{a,b,d}$	are the travel times for paths a, b, and d shown in Fig. 3;
τ_c	is the same as τ_b with reflection instead at receiver;
$\alpha_1 = \alpha_1(f,n)$	is the effective reflection coefficient for a single bounce assuming linear interaction with the surface;
$\alpha_2 = \alpha_2(f,n)$	is the reflection coefficient for a single bounce which may interact nonlinearly with the surface due to cavitation.

Note that α_2, the "nonlinear" reflection coefficient, appears only in two of the terms.

To determine if α_1 and α_2 were equal we applied the source, geometrical loss, and transfer function, to the data to compute the residual spectrum:

$$\Delta P(f,n) = P(f,n) - S(f) - G(n) - H(f,n) \tag{3}$$

for many realistic combinations of α_1 and α_2. Only when $\alpha_1 = \alpha_2$ would the ripples in the residual observed spectrum due to the near source/receiver interferences be removed correctly. This also lends credence to the assumption that the nonlinearity of the near source surface interaction is low. We also found that for all multiples the combination $\alpha_1 = \alpha_2 = -.65$ and $n = 1$ worked the best, although not perfectly. The reason for this is that for large n, say 9-24, the coefficients in front of all the exponentials in eqn. 2 are approximately equal, thus yielding a filter with very deep notches which over-corrected the observed spectra, and introduced sharp peaks in the residual spectra at the nulls of $H(f,n)$. One way to reduce the depths of the nulls was to set $n = 1$ and the α_i small so that only very incomplete cancellation could occur. This has, however, no physical justification, and it was found that the resulting uniform depth of the nulls for all frequencies at which nulls occurred was unrealistic. The observations indicated deeper nulls at low frequencies than high frequencies. In addition, the observed "residual" spectra after correction still showed quite a bit of variability and were not well "flattened" as we expected, leaving only the smooth effects of attenuation and statistical surface scattering.

The explanation for the variability of the corrected spectrum, and the changing null depth is quite simple, however, and lies in the time delays of the exponents in eqn. 2. First we approach the null width. The time delays, τ_a, τ_b, τ_c, τ_d, in eqn. 2 have the following form when the free surface is smooth and source and receiver depths are equal; $\tau \equiv (\tau_b - \tau_a) = (\tau_c - \tau_a) \approx (\tau_d - \tau_a)/2$. This leads to deep nulls in $H(f,n)$ at $f = m/\tau$, $m = \{0,1,2,\ldots\}$. However, if the four different multipaths interact n times with a surface with rms roughness σ_z, then the density function of each path length, s is approximately Gaussian, with mean given by the smooth surface value and standard deviation given in the Fraunhofer approximation [16, 17] by $\sigma_s = \sqrt{n}\, 2\sigma_z \gamma \cos\vartheta(n)$. In this relation γ is a factor which accounts for the averaging over a Fresnel zone during the interaction and is given by $\gamma = \sqrt{2}\, l / r(f,n)$ where l is the correlation length of the ice roughness and $r(f,n)$ is the Fresnel zone radius as a function of frequency and multiple. This approximation should be adequate since the Rayleigh parameter, $2k\sigma_z \cos\vartheta$, is much less than 1 for our experiment. In general, $\bar{\sigma}_z \equiv \sigma_z \gamma$ is less than σ_z due to statistical averaging over the interacting area.

If the correlation length of the surface is less than the distance between interaction points of the four multipaths, then the path lengths are statistically independent. This makes the travel times, τ_a, τ_b, τ_c, τ_d, independent, with mean given by ray theory for a smooth surface, and standard deviation, $\sigma_\tau = \sigma_s / c_0$, where where c_0 is the water sound speed at the surface. Finally, we compute the width over which the mth "null" of $H(f,n)$ should be spread by the variations in τ; $\sigma_f^m = (m/\tau^2)\,\sigma_\tau$. Since τ depends on n, and $f(n) \equiv 1/\tau(n)$, then the null width is:

$$\sigma_f^m(n) = m f^2(n) \sigma_\tau = \frac{m f^2(n) 2\sqrt{n}\,\bar{\sigma}_z}{c_0} \cos\vartheta(n). \tag{4}$$

The concept of nulls remains valid as long as σ_τ is a small fraction of the periods of the waves we are studying.

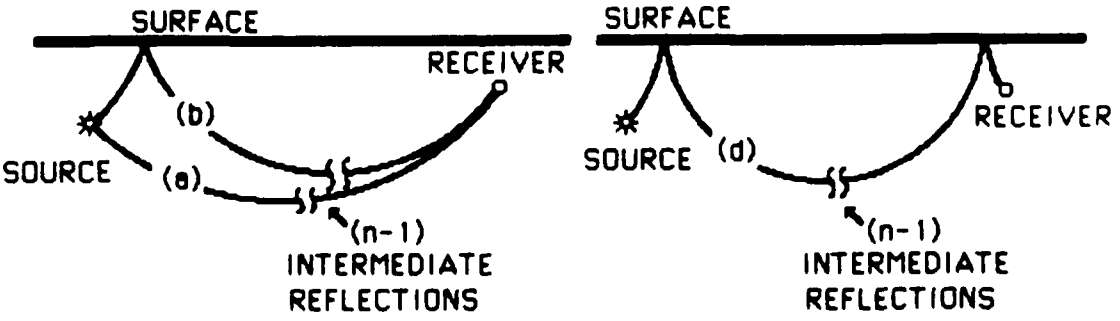

Fig. 3) Near-surface multipaths.

$$\Delta P(f,n) = P(f,n) - S(f) - G(n) - H(f,n) \tag{3}$$

for many realistic combinations of α_1 and α_2. Only when $\alpha_1 = \alpha_2$ would the ripples in the residual observed spectrum due to the near source/receiver interferences be removed correctly. This also lends credence to the assumption that the nonlinearity of the near source surface interaction is low. We also found that for all multiples the combination $\alpha_1 = \alpha_2 = -.65$ and $n = 1$ worked the best, although not perfectly. The reason for this is that for large n, say 9-24, the coefficients in front of all the exponentials in eqn. 2 are approximately equal, thus yielding a filter with very deep notches which over-corrected the observed spectra, and introduced sharp peaks in the residual spectra at the nulls of $H(f,n)$. One way to reduce the depths of the nulls was to set $n = 1$ and the α_i small so that only very incomplete cancellation could occur. This has, however, no physical justification, and it was found that the resulting uniform depth of the nulls for all frequencies at which nulls occurred was unrealistic. The observations indicated deeper nulls at low frequencies than high frequencies. In addition, the observed "residual" spectra after correction still showed quite a bit of variability and were not well "flattened" as we expected, leaving only the smooth effects of attenuation and statistical surface scattering.

The explanation for the variability of the corrected spectrum, and the changing null depth is quite simple, however, and lies in the time delays of the exponents in eqn. 2. First we approach the null width. The time delays, τ_a, τ_b, τ_c, τ_d, in eqn. 2 have the following form when the free surface is smooth and source and receiver depths are equal; $\tau \equiv (\tau_b - \tau_a) = (\tau_c - \tau_a) \approx (\tau_d - \tau_a)/2$. This leads to deep nulls in $H(f,n)$ at $f = m/\tau$, $m = \{0,1,2,\ldots\}$. However, if the four different multipaths interact n times with a surface with rms roughness σ_z, then the density function of each path length, s is approximately Gaussian, with mean given by the smooth surface value and standard deviation given in the Fraunhofer approximation [16, 17] by $\sigma_s = \sqrt{n}\, 2\sigma_z \gamma \cos\vartheta(n)$. In this relation γ is a factor which accounts for the averaging over a Fresnel zone during the interaction and is given by $\gamma = \sqrt{2}l / r(f,n)$ where l is the correlation length of the ice roughness and $r(f,n)$ is the Fresnel zone radius as a function of frequency and multiple. This approximation should be adequate since the Rayleigh parameter, $2k\sigma_z \cos\vartheta$, is much less than 1 for our experiment. In general, $\bar{\sigma}_z \equiv \sigma_z \gamma$ is less than σ_z due to statistical averaging over the interacting area.

If the correlation length of the surface is less than the distance between interaction points of the four multipaths, then the path lengths are statistically independent. This makes the travel times, τ_a, τ_b, τ_c, τ_d, independent, with mean given by ray theory for a smooth surface, and standard deviation, $\sigma_\tau = \sigma_s / c_0$, where where c_0 is the water sound speed at the surface. Finally, we compute the width over which the mth "null" of $H(f,n)$ should be spread by the variations in τ; $\sigma_f^m = (m/\tau^2)\,\sigma_\tau$. Since τ depends on n, and $f(n) \equiv 1/\tau(n)$, then the null width is:

$$\sigma_f^m(n) = m f^2(n) \sigma_\tau = \frac{m f^2(n) 2\sqrt{n}\,\bar{\sigma}_z}{c_0} \cos\vartheta(n). \tag{4}$$

The concept of nulls remains valid as long as σ_τ is a small fraction of the periods of the waves we are studying.

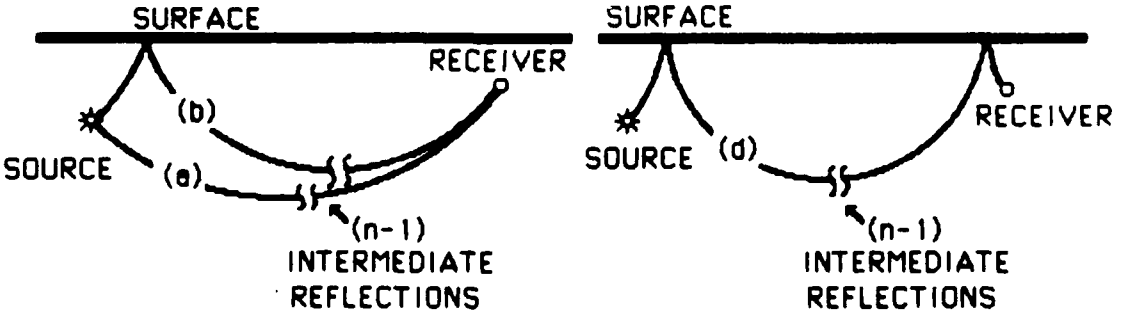

Fig. 3) Near-surface multipaths.

Equations 1 and 5 and the discussion above combine to give

$$P(f,n) = S(f) + G(n) + H(f,n) + A(f,n) \tag{6}$$

where

$$H(f,n) = n\,10\log_{10}[\,\alpha^2(f,n)\,] + 10\log_{10} < |F(f,n)|^2 > \tag{7}$$

$$= R_1(f,n) + R_2(f,n)$$

and $<|F(f,n)|^2>$ is the averaged quantity in eqn. 5. The $R_2(f,n)$ of eqn. 1 depends on the multiple order n through the τ values. $R_1(f,n)$ depends only on the scattering coefficient, $\alpha(f,n)$, thus we have separated random travel-time and scattering amplitude effects. We have parameterized the R_2 term by a single statistical quantity, σ_τ, and through it $\bar{\sigma}_z$, since travel-time variations due to sound speed effects are quite small in the Arctic[3]. It now remains to find a simple parameterization for the amplitude scattering component, $R_1(f,n)$.

The frequency dependence of the scattering term, $R_1(f,n)$ is the subject of great debate. The primary argument centers around whether Fraunhofer theories, which give the loss an f^2 dependence, or Fresnel theories, which behave as f^1[16,17] are more valid for scattering from the pack ice. For a Rayleigh parameter of $g = 2k\sigma_z\cos\vartheta \ll 1$, where k is the total wavenumber, $2\pi f/c_0$, of the insonification at the scattering boundary and ϑ is the angle of incidence, Fraunhofer theory predicts:

$$R_1(f,n) = -n\left[\,10\log_{10}(e)\,g^2(f,n) + T\,\right] \qquad \text{Fraunhofer} \tag{8}$$

T is the 2-way transmission gain at the seabottom. When g is similarly small, the first terms of the expansion for Fresnel theory predict:

$$R_1(f,n) = -n\left[\,5/2\,g(f,n) + T\,\right] \qquad \text{Fresnel} \tag{9}$$

Dyer [unpublished manuscript, 1985] indicates that observations of water column transmission loss in the Arctic are best predicted by the first term of eqn. 9. The 5/2 coefficient is close to the slope of the theoretical loss shown in Horton and Melton[16] for small Rayleigh parameter. With eqns. 8 and 9 we have a simple parameterization for the scattering loss in terms of σ_z and T.

Attenuation

In the previous section we found simple parameterizations for the transmission and scattering effects. This is also easily done for attenuation if frequency independent Q is assumed. If we are to determine the attenuation in the sediments, then loss must first be compared to that governed by dissipation in the water column. For the 9th multiple, the travel time in the water column is 233.32 seconds, and only 2.35 seconds are spent in the sediments. The attenuation coefficient for seawater is about 10^{-5} dB/km at 10 Hz and 10^{-4} dB/km at 50 Hz. The water column path length is 343 km, giving total water column losses of only 0.03 to 0.3 dB. The expected losses in the sediment are given by:

$$A(f,n) = 20\log_{10}\left[e^{\frac{-\pi f\,t(n)}{Q(n)}}\right] = -27.29\,t(n)f\;Q^{-1}(n) \tag{10}$$

where $t(n)$ is the travel-time of multiple n in the sediments and Q is the effective quality factor. We choose to solve for $Q^{-1}(n)$, the integrated effective Q^{-1} along the path for multiple n, rather than the attenuation coefficient, because there is no ambiguity in the definition of path and local slowness along the path. For multiple 9, and a Q of 200, $\alpha(10,9)$ is 0.9 dB/km, and $\alpha(50,9)$ is 4.5 dB/km. The total loss for multiple 9 is 3.2 dB at 10 Hz and 16 dB at 50 Hz. This signature is certainly observable compared to the attenuation along the water path.

Complete Model

The final modeling equation is given by:

$$\Delta P(f,n) \equiv P(f,n) - S(f) - G(n) - R_2(f,n) \tag{11}$$

$$= n \left\{ \begin{array}{l} \dfrac{-686\, f^2 \cos^2\vartheta(n)}{c_0^2}\, \sigma_z^2 \\ \dfrac{-31.4\, f \cos\vartheta(n)}{c_0}\, \sigma_z \end{array} \right\} + nT - 27.29\, t(n)\, f\, Q^{-1}(n). \qquad \begin{array}{l} \text{Fraunhofer} \\ \\ \text{Fresnel} \end{array} \qquad (11)$$

These equations will be inverted for σ_z or σ_z^2, T, and Q^{-1}. They are formally invertible for Q^{-1} as a function of n, however the conditioning for this problem is quite poor, and the issues outlined earlier make a constant Q^{-1} a more reasonable parameter to solve for.

DATA PROCESSING

Spectral Analysis

To obtain the arrival times and phase velocities of the different multiples the data were processed by a velocity analysis algorithm using the maximum-likelihood method[7] in 4 Hz bands. The results of the analysis for the first few seconds of the data are given in Fig. 5 for a center frequency of 8 Hz using a 0.25 second analysis window. The resulting stacking velocity/travel-time functions were quite similar for all frequencies in the band for the sediment arrivals. The modally dispersed water column arrivals obviously do not have this feature. The average velocity/travel-time function was used to dynamically move-out correct and stack the 22 channel data to obtain an increase in the signal to noise ratio of the bottom interacting pulses of 13.5 dB.

The stacked trace was then spectral analyzed with a tapered 0.5 second window advanced every 0.1 seconds to obtain an instantaneous energy density spectrogram. The 0.5 second window was chosen to include most of an arrival at a specific frequency in a single window for coherent addition. The combination of length and window taper gave a spectral resolution of 4 Hz, the same as the resolution of the source energy spectra computed earlier. A few seconds of the spectrogram are given in Fig. 6. The energy density of each multiple was computed by integrating in power over a small time window (1-1.5 seconds) on this spectrogram to include all the slightly dispersed arrivals which appeared in different time windows. A few examples of the observed energy density spectra $P(f,n)$ are shown in Fig. 7.

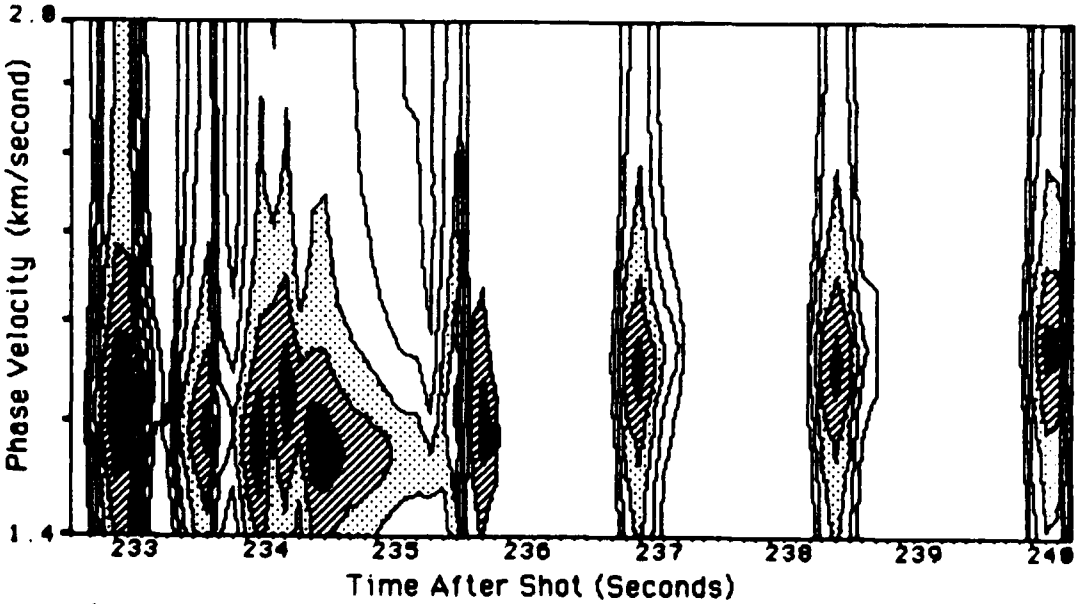

Fig. 5) Output of MLM Beamformer at 8 Hz center frequency. Contour intervals are 5 dB and are shaded with respect to local peak, not absolute level.

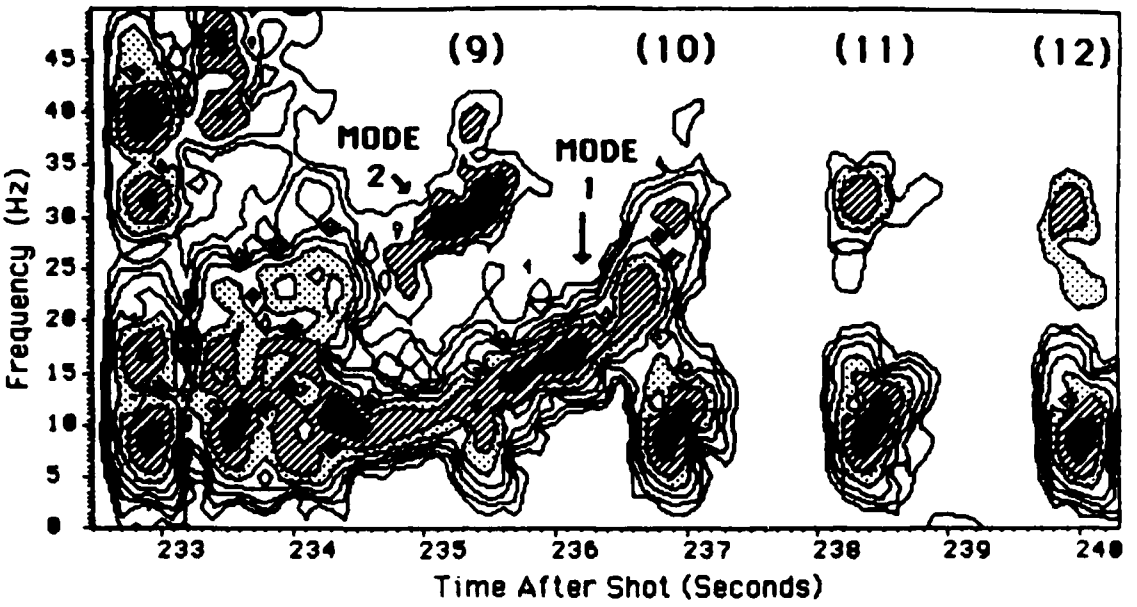

Fig. 6) Spectrogram of the stacked arrivals. Contour intervals are 5 dB, and are shaded with respect to the local peak, not absolute level. Numbers indicate order of multiple.

The ambient noise power spectrum level averaged over channels was -80 to -85 dB re 1 V^2/Hz over the 10-50 Hz band when measured on a signal free section of data before the shot. This would predict a noise energy spectral density across the band of -93 to -98 dB for multiples 9-20 with 1 second observations and -91 to -96 dB for multiples 21-24 with 1.5 second observations. These figures are a result of the array gain afforded by the 22 sensors. Note on Fig. 7 that at high frequencies and high multiple orders, the measurements are very close to the ambient noise level.

Residual Spectra

We can now compare the observations, $P(f,n)$, and the predictions given by $S(f) + G(n) + R_2(f,n)$. These are contour plotted in Fig. 8. These figures show that the locus and width of the peaks and nulls are well predicted by the statistically derived $H(f,n)$ used for R_2. We have not predicted the variations in geometrical spreading very well, as indicated by the focusing and defocusing of the power as a function of multiple in the data, but not in the predictions. These effects will, however, be diminished by the averaging over multiple order in the estimation of the attenuation and scattering. In addition, multiples 9 and 10 have some contribution from the modes that were not completely suppressed by stacking.

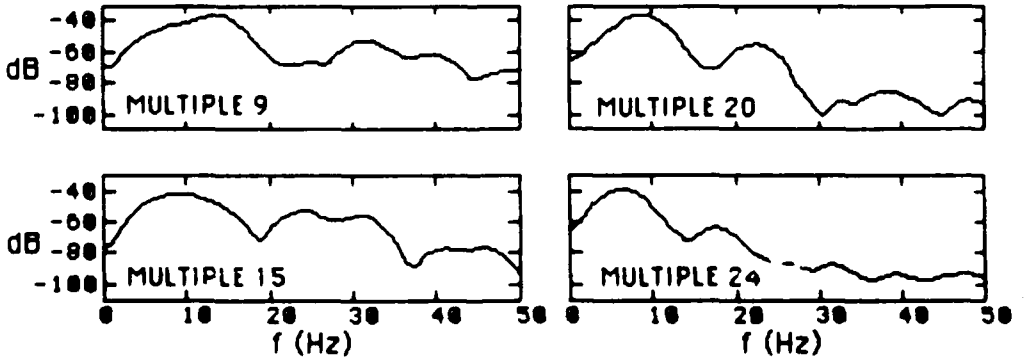

Fig. 7) Observed Energy Spectra as a function of multiple. Level is in dB re 1 V^2/Hz with -160 dB re 1 V/uPa hydrophones.

The difference between Fig. 8a and 8b should show smooth trends; i) a linear fall-off with increasing frequency for attenuation due to frequency independent Q losses, ii) a level shift downward due to frequency independent reflection or ocean bottom transmission losses, and iii) an additional frequency dependence due to surface scattering. The third term is expected to be smooth if the under-ice roughness spectrum is smooth. The variability between nearby frequencies is due to the coherent interference effects described earlier, and is unavoidable unless many realizations with different surface interaction locations are available and averaged. In addition, for high multiple orders and high frequencies, the observed spectra of Fig. 7 are very close to the ambient noise levels, even on their peaks. The "filling in" of the interfer-

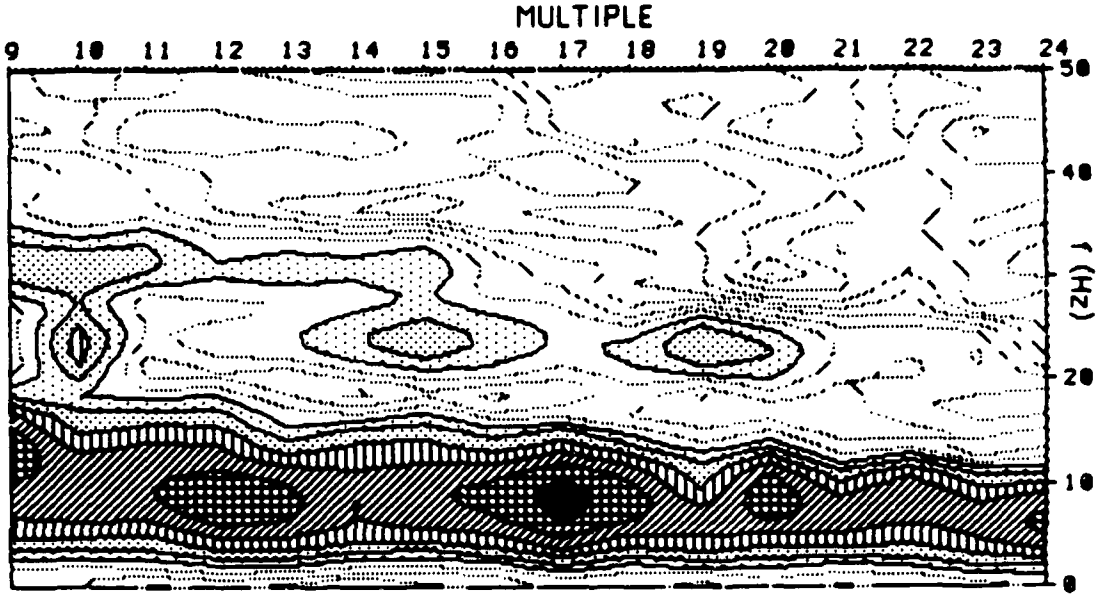

Fig. 8a) Observed energy spectrum as a function of multiple and frequency. Contour intervals are 5 dB and are shaded in absolute level.

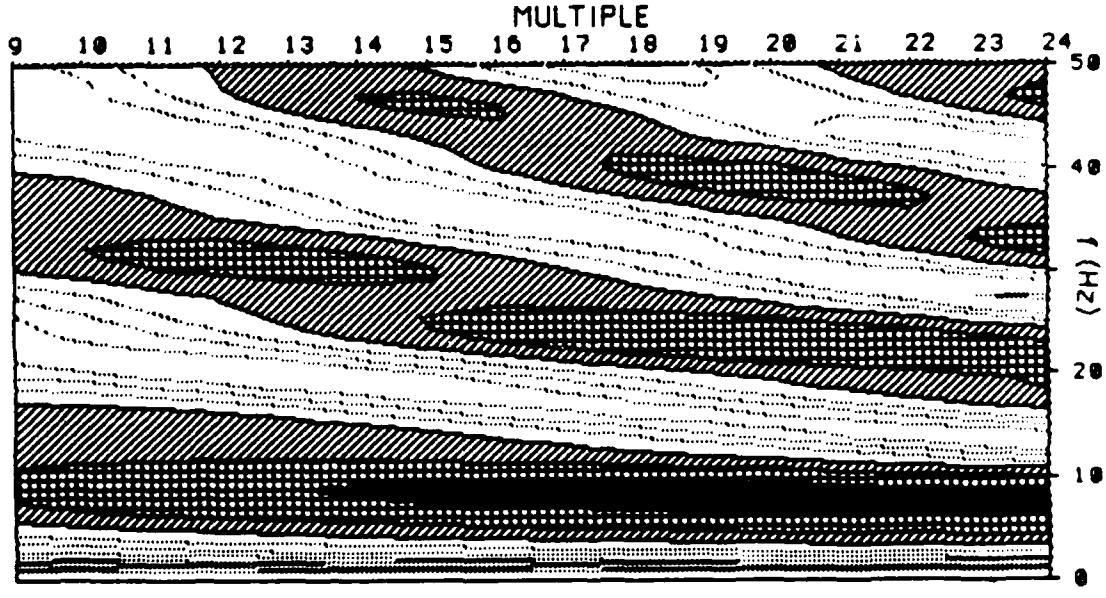

Fig. 8b) Predicted energy spectrum as a function of multiple and frequency Contour intervals and shading are the same levels as Fig. 8a. No attenuation or scattering loss has been included in the prediction

ence nulls by ambient noise are seen as artificial peaks of the residual spectra when corrected by the $R_2(f,n)$ filters. Finally, the strong modal contribution introduces an extraneous peak at 22 Hz on the residual spectrum for multiple 10.

Because errors in the R_2 spectral correction, noise, and extraneous arrivals tend to artificially increase the residual spectra, the data were edited from 832 raw spectral values to 628 and 545 values that were not felt to be corrupted. The two edited datasets were used to check the sensitivity of the parameter estimates to this possible data abuse.

INVERSION AND RESULTS

Unconstrained Inversion

The massively overdetermined systems given by eqn. 11 were solved by double-precision singular value decomposition to obtain both the estimates and the resolution and statistical properties of the inversion. The successful separation of σ_z or σ_z^2 and Q^{-1} relies on the fact that the coefficients of these terms in eqn. 11 behave differently with n, especially in the Fresnel case where linear dependence on f is expected for both terms. Unfortunately, $n\cos\vartheta(n)$ and $t(n)$ both have similar behavior. While the resolution was perfect with condition numbers of 10^5 in the Fraunhofer case and 10^3 in the Fresnel case, the correlation coefficient between σ_z^2 and Q^{-1} was -.962. In the Fresnel case, the value was -.986. For the 545 point dataset, the parameters which give the minimum rms error fit to the data are given below.

Theory	T (dB)	σ_z (meters)	Q	rms error (dB)
Fraunhofer	$-.318\pm.008\ \sigma_p$	$4.09\pm.06\ \sigma_p$	$2865\pm614\ \sigma_p$	4.32
Fresnel	$.21\pm.005\ \sigma_p$	$11.0\pm.13\ \sigma_p$	$-208\pm5.4\ \sigma_p$	3.89

Although the spectral data are certainly non-Gaussian, we still deal only with 2nd moment statistics. σ_p is the standard deviation of the data spectral values, and may be approximated by the rms error. Both of these results are clearly unrealistic, the Fraunhofer yielding an rms roughness that is too large, and a Q that is too high, and the Fresnel yielding a negative Q (energy gain!) and a roughness that is too large in order to compensate for the negative Q. Allowing T to vary with n to compensate for geometrical spreading correction errors did not change the results significantly.

Constrained Inversion

Because Q and σ_z co-vary so strongly, it was felt that σ_z might be constrained by the travel-time variance measurements inferred from the $R_2(f,n)$ filters given earlier, and σ_z calculated from it and the Fresnel zone averaging term, $\gamma = \sqrt{2}\,l/r(f,n)$. We have not formally inverted the spectra for $\sigma_\tau(f,n)$ since this would require much more stable data spectral estimates than we have for this single shot. However, it is possible to use the theory developed for $R_2(f,n)$ and geometrical optics to calculate $\gamma(f,n)$ to obtain σ_z from the spectral shapes. To illustrate this procedure using the measured value of σ_τ = 1 msec, and σ_z = 2.5 meters, we obtain $\gamma(f,9) = 1/4$, $\gamma(f,16) = 1/6$, and $\gamma(f,24) = 1/10$ assuming a correlation length of 20 meters [18]. This gives Fresnel radii of 100, 170, and 280 meters, respectively for multiples 9, 16, and 24. These are quite comparable to the normal incidence Fresnel radius for a homogeneous water column at 20 Hz with a depth of h =4 km of $r=\sqrt{\lambda h/2}$ = 400 meters. We use 20 Hz because the nulls near this frequency were modeled most accurately by σ_τ=1 msec. Note that as the higher multiples approach normal incidence, the agreement is better.

Because the single shot data do not allow an unconstrained separation of the Q and scattering contributions using the current formulation, we plot the tradeoff curve for σ_z and Q in which Q is varied as a constraint and σ_z and T are chosen to minimize the rms data fitting error. This gives a region of acceptable results to which one can apply their personal bias, Q implying σ_z and vice versa. This is illustrated in Fig. 9a. We feel that these results constrain Q to lie from 200 to 300. The rms error curves are quite flat for these estimates, and are shown in Fig. 9b. We feel that the current inversion is inadequate to distinguish between the Fresnel and Fraunhofer theories. The Fraunhofer result is attractive because its rms error is closer to the unconstrained value at the physically feasible solutions. However, the constrained solutions for both are quite similar, and the constrained Fraunhofer predictions fall off nearly as linearly with frequency as the Fresnel since they are strongly controlled by the attenuation term. The 545 point data set and predictions for selected multiples are given in Fig.

10. It should also be noted that a cubic polynomial in place of the scattering theories had almost the same minimum rms error as the best fit values of Fig. 11, indicating that a model with more degrees of freedom, but still smooth, is not the solution to the problem. The Q predicted by this method was 393.

CONCLUSIONS

The disparity between the best fit parameter standard deviations and their feasible values indicates that the loss model in the inversion has not yet been parameterized correctly. This is also indicated by the extremely flat rms fitting error curve with large minimum value at the best solution (Fig. 9b). It is felt that the correct parameterization will include the $R_2(f,n)$ term directly in the inverse problem. Since this is a nonlinear term in the parameter $\bar{\sigma}_z(f,n)$, it will require a more complicated inversion procedure. This was not carried out for this work because it does not make sense to

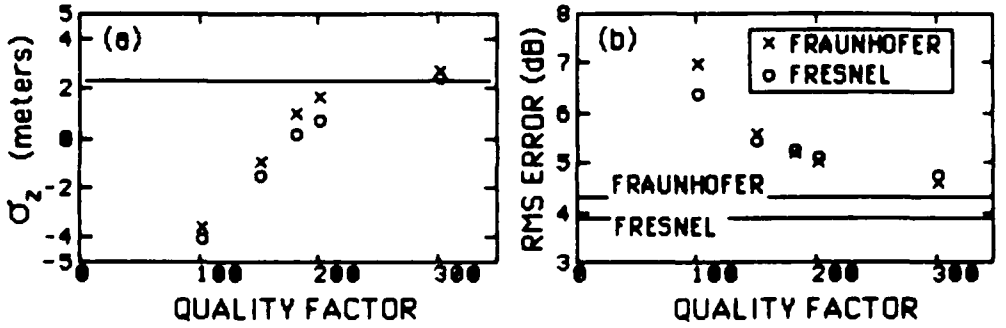

Fig. 9) (a) Estimated rms surface roughness as a function of Q. Line at 2.3 meters shows accepted value for Arctic. (b) RMS fitting error as a function of Q constraint value. Lines give minimum errors of unconstrained problem.

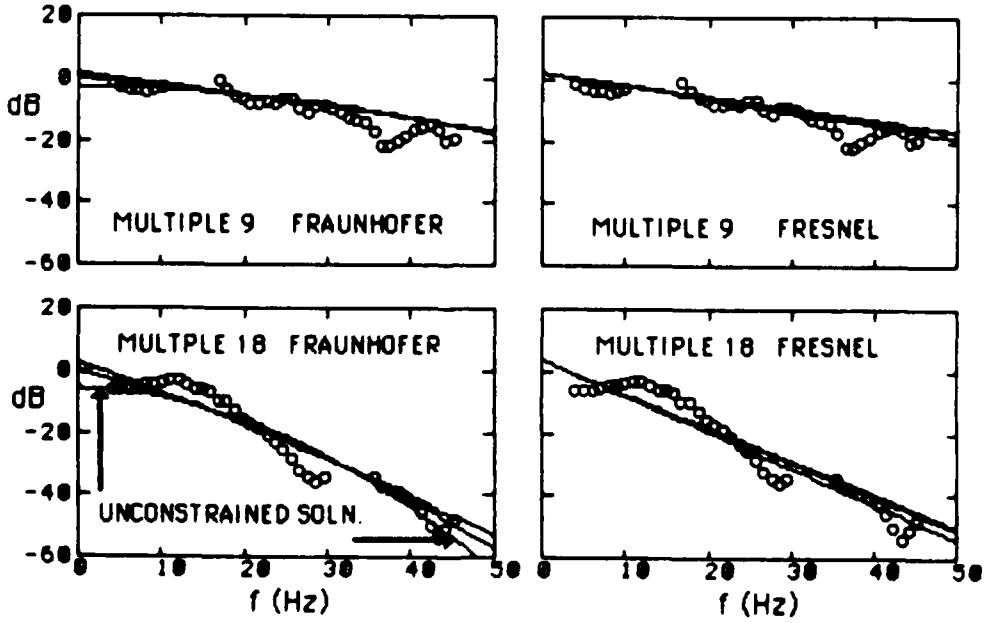

Fig. 10) Sample spectra from edited dataset (o labels) and fits of minimum RMS error, Q=200 and Q=300 constrained solutions.

invert data which are not ergodic, and are only one realization of the process, for this statistical parameter. For this work we have chosen the most smoothed parameters that would yield scientifically interesting answers, but still found the data somewhat inadequate. Future work will include improving the dataset by averaging, and inclusion of the coherent part of the scattering process directly in the inversion procedure. The separation of scattering and attenuation will also be greatly improved by utilizing the modal arrivals which do not interact with the ocean bottom.

We feel that the constrained inversion results indicate a very high sediment Q of 200 to 300 for the upper 200 meters. This value is consistent with the work of Lee [4] which reported values ranging around 200 when scattering was neglected, thus biasing his results downward. Helmberger, et al., [14] report Q values of 500 for similar sediments in the Bering Sea. We note that Q estimates are very sensitive to surface roughness assumptions in the range of roughnesses reported for the Arctic.

Finally, we have shown that partially coherent summation of travel paths is required to predict the magnitude and shape of the observed spectral functions. For this region, we also note that about half of the energy observed after 340 km of propagation has interacted with the ocean bottom, and all of it has interacted with the ice, making the separation of these effects very important to understanding propagation in this region.

ACKNOWLEDGEMENTS

The authors wish to thank Ira Dyer and Wafic Beydoun for their helpful discussions. This work was supported by the Office of Naval Research, Arctic Programs Office under contract #N 00014-77-C-0266.

1. R.D. Stoll, "Marine sediment acoustics," *J. Acoust. Soc. Am.* **77**(5) pp. 1789-1799 (1985).
2. R.D. Stoll and Houtz, R.E., "Attenuation measurement with sonobuoys," *J Acoust. Soc. Am.* **73**(1) pp. 163-172 (1983).
3. Mikhalevsky, P.N., "Characteristics of CW signals propagated under the ice in the Arctic," *Journal of the Acoustical Society of America* **70**(6) pp. 1717-1722 (1981).
4. Lee, T., "Long-range sound transmission of bottom-interacting signals in the Arctic channel: Experiment and theory," Ph.D. Thesis, Columbia University, University Microfilms International, Ann Arbor, MI (1983).
5. Hamilton, E.L., "Prediction of in situ acoustic and elastic properties of marine sediments, North Pacific," *Geophysics* **36** pp. 266-284 (1971).
6. Hamilton, E.L., "Geoacoustic modeling of the sea floor," *J Acoust Soc Am* **68** pp. 1313-1340 (1980).
7. Duckworth, G.L., Baggeroer, A.B., and Jackson, H.R., "Crustal Structure Measurements near FRAM II in the Pole Abyssal Plain," *Tectonophysics* **89** pp. 172-215 (1982).
8. Wakeley, J., "Pressure-signature model for an underwater explosive charge," *U.S. Navy Journal of Underwater Acoustics* **27**(2) pp. 445-449 (1977).
9. Urick, R.J., *Principles of Underwater Sound*, McGraw-Hill Book Co., New York, NY (1975).
10. R.S. Jacobson, G.G.Shor, Jr., and Dorman, L.M., "Linear inversion of body wave data - part II: Attenuation versus depth using spectral ratios," *Geophysics* **46** pp. 84-94 (1981).
11. Duckworth, G.L., *Processing and Inversion of Arctic Ocean Refraction Data*, Sc.D. Thesis, Massachusetts Institute of Technology; Department of Electrical Engineering and Computer Science; Woods Hole Oceanographic Institution; Department of Oceanographic Engineering (September, 1983).
12. Diebold, J.B. and Stoffa, P.L., "The traveltime equation, tau-p mapping, and inversion of common midpoint data," *Geophysics* **46**(3) pp. 238-254 (1981).
13. Dorman, L. and Jacobson, R.S., "Linear Inversion of Body Wave Data; Part I: Velocity Structure From Travel Times and Ranges," *Geophysics* **46**(2) pp. 138-151 (1981).
14. D.V. Helmberger, G. Engen, and Scott, P., "A note on velocity, density and attenuation models for marine sediments determined from multi-bounce phases," *J Geophys. Res.* **84** pp. 667-671 (1979).
15. Weston, D.E., "Underwater Explosions as Acoustic Sources," *Proceedings of the Physical Society* **76** p. 233 (1960).

16. Horton, C.W. Sr. and Melton, D.R., "Importance of the Fresnel Correction in Scattering from a Rough Surface. II. Scattering Coefficient," *Journal of the Acoustical Society of America* **47**(1) pp. 299-303 (1970).
17. Melton, D.R. and Horton, C.W. Sr., "Importance of the Fresnel Correction in Scattering from a Rough Surface. I. Phase and Amplitude Fluctuations," *Journal of the Acoustical Society of America* **47**(1) pp. 290-298 (1970).
18. Mellen, R.H. and Dinapoli, F.R., "Underwater Acoustics in the Arctic Ocean," *NATO Advanced Study Institute on Adaptive Methods in Underwater Acoustics*, (1984).